Seismic Detection of the Lunar Core

Renee C. Weber,[1]* Pei-Ying Lin,[2] Edward J. Garnero,[2] Quentin Williams,[3] Philippe Lognonné[4]

Despite recent insight regarding the history and current state of the Moon from satellite sensing and analyses of limited Apollo-era seismic data, deficiencies remain in our understanding of the deep lunar interior. We reanalyzed Apollo lunar seismograms using array-processing methods to search for the presence of reflected and converted seismic energy from the core. Our results suggest the presence of a solid inner and fluid outer core, overlain by a partially molten boundary layer. The relative sizes of the inner and outer core suggest that the core is ~60% liquid by volume. Based on phase diagrams of iron alloys and the presence of partial melt, the core probably contains less than 6 weight % of lighter alloying components, which is consistent with a volatile-depleted interior.

Recent studies suggest that the Moon possesses a relatively small iron-rich core, sized between ~250 and 430 km, or roughly 15 to 25% of its 1737.1-km mean radius (*1*). Various indirect geophysical measurements provide supporting evidence for the presence of a core (*1*–*4*), but differ on key characteristics such as its radius, composition, and state (solid versus molten), although a liquid core is favored when considering Love numbers (*3*) or mantle seismic constraints (*5*). Constraining the structure of the lunar core is necessary for understanding the present-day internal thermal structure, the history of a lunar dynamo, and the origin and evolution of the Moon (*1*).

Seismic models of the lunar interior lack resolution in the deepest 500 km of the Moon (*6*–*9*), because of the paucity of seismic waves that penetrate this depth range identified in the Apollo seismic data. The lack of observation of far-side events recorded by the nearside array suggests the presence of a highly attenuating region in the deep Moon (*10*). This, combined with inferences from other geophysical data (*1*), has led to a model containing a partially molten deepest mantle layer overlying molten outer and solid inner core layers (Fig. 1A).

The Apollo Passive Seismic Experiment (PSE) consisted of four seismometers deployed on the lunar nearside between 1969 and 1972, which continuously recorded three orthogonal directions of ground motion until late 1977. The small number of stations, limited selenographical extent of the network, and weak attenuation of seismic energy coupled with strong wave scattering prohibited direct observation of waves reflected off of or refracted through the core.

We applied seismic array-processing methodologies to the PSE data to search for layering in the deep Moon that might be associated with a lunar core (*11*, *12*). We analyzed seismograms from previously identified deep moonquakes (*10*), which are the most abundant type of lunar seismic events. They are known to originate from discrete kilometer-scale source regions (*13*) or

[1]NASA Marshall Space Flight Center, 320 Sparkman Drive, Huntsville, AL 35805, USA. [2]School of Earth and Space Exploration, Arizona State University, Tempe, AZ, USA. [3]Department of Earth and Planetary Sciences, University of California Santa Cruz, Santa Cruz, CA, USA. [4]Institut de Physique du Globe–Sorbonne Paris Cité, Université Paris Diderot, Saint-Maur-des-Fosses, France.

*To whom correspondence should be addressed. E-mail: renee.c.weber@nasa.gov

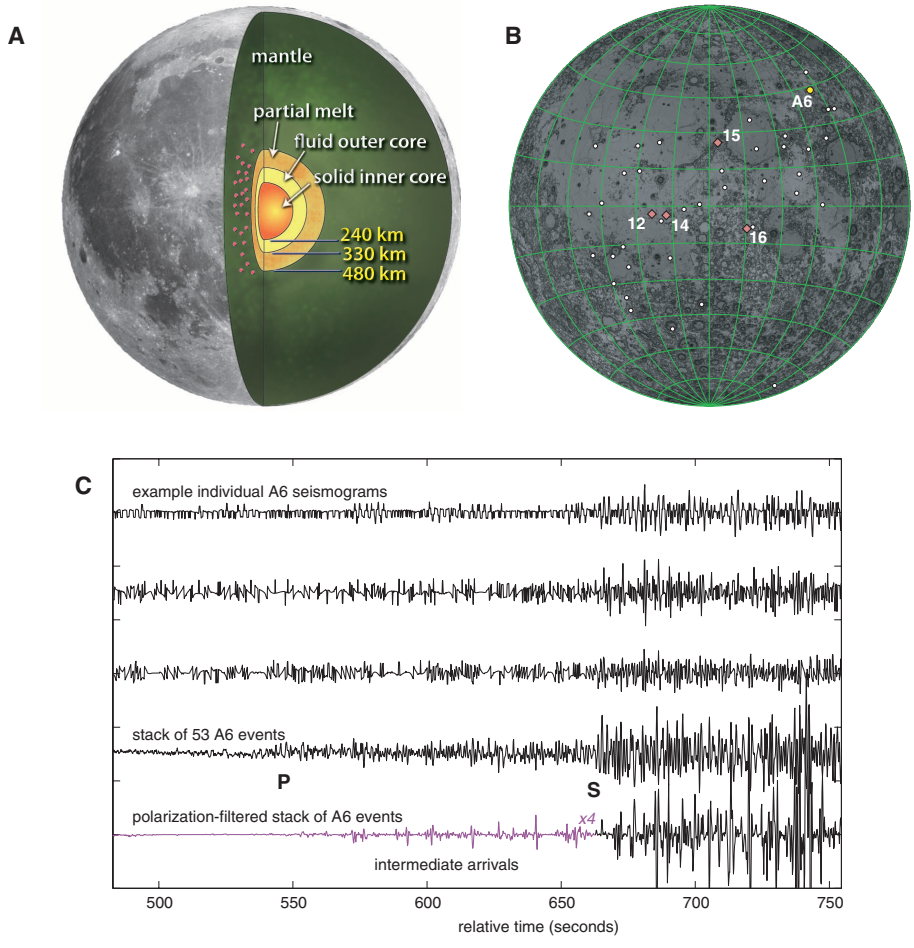

Fig. 1. (**A**) Schematic meridional cross-section of the Moon showing the distribution of deep moonquakes (red circles) and the potential radii of physical layers in the deepest lunar interior. (**B**) Map of the lunar nearside showing the locations of the Apollo seismic stations (red diamonds) and the distribution of the deep moonquake epicenters used in this study (white circles). (**C**) The *R*-component seismograms of station 15 from three A6 events (top three traces), compared to a stack of A6 events on the *R* component of station 15 (fourth from top), and the same stack after polarization filtering (bottom). The *P* arrival is not evident in the single-event seismograms, because amplitudes of a single digital unit, reflecting the noise floor of the instrument, dominate the traces before the *S* arrivals. Stacking enhances the *P* and *S* arrivals, but intermediate arrivals remain masked by the *P*- and *S*-wave codas. The polarization filter reveals arrivals between *P* and *S*. We multiplied the segment of the seismogram before *S* (highlighted in purple) by a factor of 4 to increase the visibility of the intermediate arrivals.

"clusters" (Fig. 1B), with depths between 700 and 1200 km. Clusters produce repeatable seismic waveforms at each station, permitting seismogram stacking to improve the signal-to-noise ratio of the main *P*- and *S*-wave arrivals (*14*). However, scattering effects presumed to originate in the lunar crust persist, manifesting as long, ringing codas on all three components of ground motion that obscure subtle arrivals that may be associated with deep interfaces (Fig. 1C).

We suppressed coda noise with a polarization filter, a time-averaged product between orthogonal components of motion, which enhances signals partitioned onto more than one component (*12*). Polarization filtering enhances the main *P*- and *S*-wave arrivals and reveals a number of intermediate arrivals (Fig. 1C). Array-processing methods commonly used in terrestrial seismology (*11*) permit investigation of deep layering as the source of these arrivals. Stacking seismograms that have been aligned on predicted core arrival times enhances small-amplitude arrivals. We searched for lunar core reflections by time-shifting the polarization-filtered deep moonquake cluster stacks to travel time predictions of reflections from specific layer depths, then summing the shifted traces. If relatively strong energy is present in a stack associated with a particular depth, this is evidence for a reflective boundary at that depth.

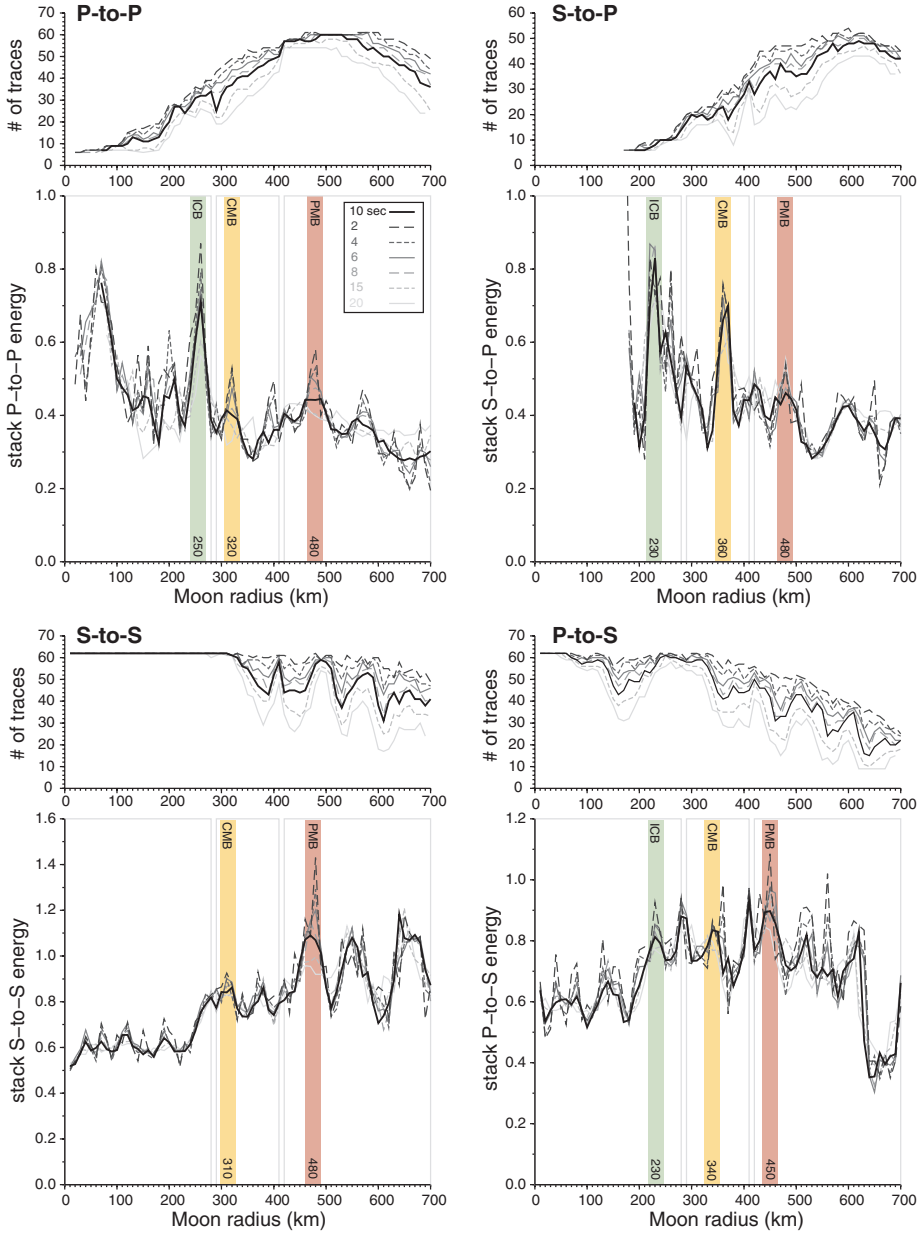

Fig. 2. For the four types of reflections (*P*-to-*P*, *S*-to-*S*, *S*-to-*P*, and *P*-to-*S*), the area under each stack (a proxy for energy) is plotted against the core radius, for each of the stack window lengths under consideration (bottom curves). We highlight the 10-s window (bold line), although no specific window length was given any greater weight in our interpretation. We normalized the value at each radius increment by the number of traces contributing to the stack (top curves). Gray lines demarcate the depth regions over which each interface was iteratively searched. Model interface depths are highlighted in green (ICB), yellow (CMB), and pink (PMB), and vary because of uncertainties in velocity structure and variable (sometimes low) numbers of stacked records. Supporting data relevant to the significance of each peak are shown in fig. S5 (*12*).

Array seismology techniques are commonly performed relative to a reference signal, to suppress event origin errors. The direct *S* wave is the largest arrival on the cluster-stacked moonquake traces, and thus we used it as a reference phase by hand-picking *S*-wave arrival onset times (*12*). We began with stacks of seismograms (*14*) recorded on the four Apollo stations from all 106 located clusters, retaining data only for which *S*-wave onsets were clear and impulsive, resulting in 62 picks from a total of 38 clusters (table S1).

A number of distinct interfaces (Fig. 1A) could reflect seismic energy from deep moonquakes back to the surface. We searched the PSE data for four distinct reflection types: (i) a downward-propagating *P* wave that reflects and travels up to the surface as a *P* wave; (ii) as in (i), but a down- and upgoing *S* wave, horizontally polarized as *SH*; (iii) a downward-propagating *S* wave that converts to *P* upon reflection, traveling up as a *P* wave; (iv) a downward-propagating *P* wave that converts to *S* upon reflection, returning as an *S* wave. The *S* waves in cases (iii) and (iv) are vertically polarized shear waves (*SV*). We explored layered models (Fig. 1A) in which we expect reflections off of the following: the partial melt boundary (PMB, interface *d*; for example, a *P*-to-*P* reflection is named *PdP*), the outer fluid core or core-mantle boundary (CMB, interface *c*; for example, *PcP* for *P*-to-*P* reflections), and the inner core boundary (ICB, interface *i*; for example, *PKiKP* for *P*-to-*P* reflections).

To detect deep reflections, we computed the envelope of the stack associated with each depth increment and computed the area under the curve (Fig. 2). We made stacks for all four wave types (*12*), with time-window lengths varying from 2 to 20 s, centered on the predicted reflection arrival time (to allow for possible moonquake origin time and location errors). Double-array stacking for models with multiple layering (Fig. 1A) involves an iterative approach that seeks the best-fit radii and overlying *P*- and *S*-wave speeds of each layer, in order to produce consistency in the stacks for the four wave types (*P*-to-*P*, *S*-to-*S*, *S*-to-*P*, and *P*-to-*S*). We stacked data one interface at a time, because resolving deeper interfaces requires knowledge of overlying structure.

We adopted the approach of interpreting peaks in Fig. 2 that were common to the different wave-type stacks, with relatively high record counts. A layer near 480 ± 15 km radius (*12*) is coherent in the stacks, after a slight (5% increase) perturbation in *P* velocities immediately above the PMB. We used a compressional wave velocity of 8.5 km/s between 738 and 1257 km depth: This velocity likely requires the presence of garnet (at the ~20% level) at depth in the lunar mantle, which has been suggested previously (*1*, *9*). Lower velocities (and hence lower

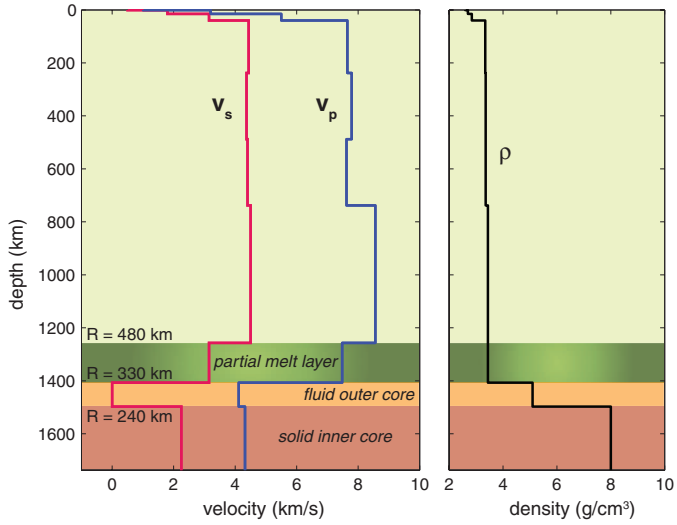

Fig. 3. Preferred velocity (v) and density (ρ) models. Structure shallower than 1000 km is derived from previous studies (*7*, *8*), whereas that within the core is derived from the elasticity of iron alloys (*16*, *21*, *26*).

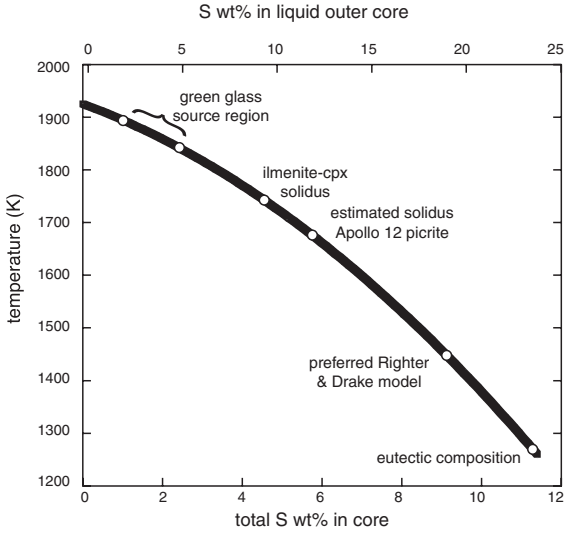

Fig. 4. Tradeoff between the sulfur content of the lunar core and the liquidus temperature. The inner core is assumed to be pure iron, in accord with the eutectic behavior of the Fe-FeS system. Available solidus temperatures at lunar CMB pressures of anhydrous compositions relevant to the overlying partially molten zone, such as the Apollo 12 12009 picrite (*22*), ilmenite-clinopyroxene cumulates (*23*), and the green glass source region (*24*), are also shown, as is an estimate of the sulfur composition of the lunar core derived from siderophile element abundances (*27*). The phase diagram for the Fe-S system at 5 GPa is interpolated between the ambient-pressure phase diagram, the results of (*28*) at 3 Gpa, and those of (*29*) at 10 GPa. The densities of liquids in the Fe-S system are derived from elastic parameters from (*16*, *26*). For comparison, if an equal mixture of carbon and sulfur by weight were present [such as a mix of 5 weight % (wt %) carbon and 5 wt % sulfur in place of 10 wt % sulfur], the liquidus temperature would be lowered by ~100 K across much of this compositional range, and immiscible liquids would be unlikely to occur at the pressure of the lunar core (*30*).

amounts of garnet) are permissible as well, but produce slightly less robust stacks (*12*). We assign the layer of partial melt between the PMB and CMB with P and S velocity reductions of 10 and 30%, respectively (*15*), corresponding to ~5 to 30% partial melt at depth, with the amount depending on whether the liquid is distributed in isolated pockets or tubes (~30%) or is present as intergranular films (~5%: presumed to be 100:1 aspect ratio; lower aspect ratios imply greater melt percentages). In the former instance, the amount of melt lies below the percolation threshold; the latter scenario would imply that the melt is either neutrally buoyant or, less plausibly, dynamically entrained in the lunar mantle. Although these reductions are assumed, they do represent velocity contrasts that are physically reasonable, will produce notable attenuation observed for deeply sampling seismic phases, are detectable, and are compatible with the lack of observed deep moonquakes below 1200 km depth (*10*). The sharp onset of the PMB and its coherence at a single depth imply that lunar mantle material intersects its solidus at this depth, and that lateral temperature gradients in the deep mantle may be small. After fixing the PMB depth and velocities, the best-fitting CMB radius is determined to be 330 ± 20 km. We adopt a fluid outer core P velocity of 4.1 km/s, which is consistent with a liquid iron alloy under these conditions (*16*), resulting in a strong reflection near 240 ± 10 km radius. This deep discontinuity, which lacks *SH* reflections (Fig. 2), is most readily associated with a solid inner core. A transition from liquid to solid at this location implies that the Moon's core is ~40% solidified.

The different wave types and resultant preferred velocity model show consistent evidence for a PMB, CMB, and ICB (Fig. 3 and table S2). The seismic velocities we have assumed for our core layers are consistent with estimates from other studies (*17*). However, these velocity assumptions affect the modeled reflector depths, because the depth of any reflector has a 1-to-1 tradeoff with the velocity above the interface. Continued model velocity adjustment might result in better peak alignment between the different stacks, but the choice of velocity is not well constrained at present. Our principal results, motivated by consistencies in the stacks of different data types, demonstrate the strength of the deep reflectors and strongly suggest that the Moon has a solid inner and fluid outer core, overlain with a partially molten layer. Layer depths may plausibly vary by tens of kilometers; the exact resolution is difficult to quantify, owing to uncertainties such as moonquake location and timing errors, seismic heterogeneities that either blur stack amplitudes or affect one wave type more than another (such as the CMB in the *S*-to-*P* stack), and fairly low record numbers for some depth regions for some wave types. We thus emphasize the qualitative agreement between the different types of reflected waves, which is excellent given the original ringy PSE data.

The relative amplitudes of peaks in our stacks might suggest relative strengths of impedance contrasts of the various boundaries. However, a number of uncertainties preclude this, including the unknown radiation patterns of *P*, *SV*, and *SH* energy; the sharpness of interfaces; and the effects of heterogeneity on the different wave types. Nonetheless, these results provide a seismic constraint on deep lunar structure against which other types of geophysical data can be tested. Among those, moment of inertia, density, and the tidal Love numbers are the most sensitive to the core. We therefore test our model against the tidal Love numbers k_2 and h_2 obtained from lunar laser ranging.

The accepted values are $k_2 = 0.0209 \pm 0.0025$ and $h_2 = 0.041 \pm 0.008$ (*18*). Satellite tracking data provide a similar value for k_2, although with a larger uncertainty ($k_2 = 0.0213 \pm 0.0075$) (*19*). Both of these estimates are significantly smaller than those proposed by (*20*), with $k_2 = 0.026 \pm 0.003$. If we assume densities of 5.1 g/cm^3 and 8.0 g/cm^3 in the outer and inner core respectively, corresponding to the seismic velocities we proposed for iron cores (*12*), we obtain k_2 and h_2 equal to 0.0232 and 0.0406, respectively. Thus, our proposed model predicts k_2 within slightly less than 1 SD of the value predicted from laser ranging, which is close to the average of (*18*) and (*20*).

A conservative interpretation of our deep reflections is that the deepest interior of the Moon has considerable structural similarities with Earth: Constraints on temperature in the lunar interior can be derived from the depth of the ICB, coupled with the phase diagram of plausible iron alloys. The tradeoffs between the amount of sulfur within an iron-sulfur core and the temperature at its ICB (Fig. 4) indicate that the ICB temperature is probably within tens of kelvin of that at the CMB. This is a consequence of the Moon's

liquid outer core being subadiabatic and probably stably stratified. Such stable stratification is a natural consequence of the adiabat of iron alloys probably being steeper than their liquidus at lunar core conditions (*21*) and is consistent with the present absence of a lunar dynamo. An attenuating, probably partial melt-bearing layer at the base of the mantle provides a constraint on the thermal regime and hence on core chemistry. Characteristic estimates of the anhydrous solidi of possible lunar mantle materials at lowermost mantle pressures typically lie above ~1650 K (*22*–*24*). Therefore, the solidi temperatures imply that the sulfur content within the lunar outer core is ~6 weight % or less (Fig. 4). If significant water is present at depth in the deep Moon, then solidus temperatures would be lowered in the partially molten zone, and somewhat higher sulfur contents would be permitted. The depletion in lighter alloying components relative to Earth's core is consistent with depletion of the lunar interior in volatile elements relative to Earth. Such depletion is a natural consequence of the lunar formation process, through high-temperature devolatilization during the Moon-forming impact: In effect, the present lunar core is probably composed of thermally processed material from the core of the impactor (*25*).

References and Notes

1. M. A. Wieczorek *et al.*, *Rev. Mineral. Geochem.* **60**, 221 (2006).
2. A. S. Konopliv, A. B. Binder, L. L. Hood, W. L. Kucinskas, J. G. Williams, *Science* **281**, 1476 (1998).
3. J. G. Williams, D. H. Boggs, C. F. Yoder, J. T. Ratcliff, J. O. Dickey, *J. Geophys. Res.* **106**, 933 (2001).
4. L. L. Hood, D. L. Mitchell, R. P. Lin, M. H. Acuna, A. B. Binder, *Geophys. Res. Lett.* **26**, 2327 (1999).
5. P. Lognonné, C. Johnson, *Treatise Geophys.* **10**, 69 (2007).
6. Y. Nakamura, *J. Geophys. Res.* **88**, 677 (1983).
7. P. Lognonné, J. Gagnepain-Beyneix, H. Chenet, *Earth Planet. Sci. Lett.* **211**, 27 (2003).
8. J. Gagnepain-Beyneix, P. Lognonné, H. Chenet, D. Lombardi, T. Spohn, *Phys. Earth Planet. Inter.* **159**, 140 (2006).
9. A. Khan, J. A. D. Connolly, J. Maclennan, K. Mosegaard, *Geophys. J. Int.* **168**, 243 (2007).
10. Y. Nakamura, *J. Geophys. Res.* **110**, E01001 (2005).
11. S. Rost, C. Thomas, *Rev. Geophys.* **40**, 1008 (2002).
12. Methods are available as supporting material on *Science* Online.
13. Y. Nakamura, *Proc. Lunar Planet. Sci. Conf. 9th* **3**, 3589 (1978).
14. R. C. Bulow, C. L. Johnson, P. M. Shearer, *J. Geophys. Res.* **110**, E10003 (2005).
15. Q. Williams, E. J. Garnero, *Science* **273**, 1528 (1996).
16. C. Sanloup *et al.*, *Geophys. Res. Lett.* **27**, 811 (2000).
17. Y. Nakamura *et al.*, *Geophys. Res. Lett.* **1**, 137 (1974).
18. J. G. Williams, D. H. Boggs, J. T. Ratcliff, paper presented at the 41st Lunar and Planetary Science Conference, The Woodlands, TX, 1 to 5 March 2010. Sponsored by the Lunar and Planetary Institute.
19. S. Goossens, K. Matsumoto, *Geophys. Res. Lett.* **35**, L02204 (2008).
20. A. S. Konopliv, S. W. Asmar, E. Carranza, W. L. Sjogren, D. N. Yuan, *Icarus* **150**, 1 (2001).
21. Q. Williams, *Earth Planet. Sci. Lett.* **284**, 564 (2009).
22. D. H. Green, N. G. Ware, A. J. Hibberson, W. O. Major, *Earth Planet. Sci. Lett.* **13**, 85 (1971).
23. B. A. Wyatt, *Contrib. Mineral. Petrol.* **61**, 1 (1977).
24. J. Longhi, *Geochim. Cosmochim. Acta* **70**, 5919 (2006).
25. R. M. Canup, *Icarus* **168**, 433 (2004).
26. P. S. Balog, R. A. Secco, D. C. Rubie, D. J. Frost, *J. Geophys. Res.* **108**, 2124 (2003).
27. K. Righter, M. J. Drake, *Icarus* **124**, 513 (1996).
28. R. Brett, P. M. Bell, *Earth Planet. Sci. Lett.* **6**, 479 (1969).
29. B. Chen, J. Li, S. A. Hauck II, *Geophys. Res. Lett.* **35**, L07201 (2008).
30. R. Dasgupta, A. Buono, G. Whelan, D. Walker, *Geochim. Cosmochim. Acta* **73**, 6678 (2009).

31. This work was funded by NASA Planetary Geology and Geophysics grant NNH09AK41I to R.C.W. The authors thank four reviewers, and Y. Nakamura for helpful comments and discussions.

Supporting Online Material

www.sciencemag.org/cgi/content/full/science.1199375/DC1
SOM Text
Figs. S1 to S7
Tables S1 and S2
References

21 October 2010; accepted 16 December 2010
Published online 6 January 2011;
10.1126/science.1199375

A Persistent Oxygen Anomaly Reveals the Fate of Spilled Methane in the Deep Gulf of Mexico

John D. Kessler,[1]* David L. Valentine,[2]* Molly C. Redmond,[2] Mengran Du,[1] Eric W. Chan,[1] Stephanie D. Mendes,[2] Erik W. Quiroz,[3] Christie J. Villanueva,[2] Stephani S. Shusta,[2] Lindsay M. Werra,[2] Shari A. Yvon-Lewis,[1] Thomas C. Weber[4]

Methane was the most abundant hydrocarbon released during the 2010 Deepwater Horizon oil spill in the Gulf of Mexico. Beyond relevancy to this anthropogenic event, this methane release simulates a rapid and relatively short-term natural release from hydrates into deep water. Based on methane and oxygen distributions measured at 207 stations throughout the affected region, we find that within ~120 days from the onset of release ~3.0×10^{10} to 3.9×10^{10} moles of oxygen were respired, primarily by methanotrophs, and left behind a residual microbial community containing methanotrophic bacteria. We suggest that a vigorous deepwater bacterial bloom respired nearly all the released methane within this time, and that by analogy, large-scale releases of methane from hydrate in the deep ocean are likely to be met by a similarly rapid methanotrophic response.

The immense accumulation of methane (CH_4) in the marine sub-seafloor is among the largest global carbon reservoirs (*1*) and has been implicated as a factor in past oceanic and climate change. Oceanic CH_4 released naturally through hydrocarbon seeps, hydrothermal vents, or decomposing clathrate hydrates or anthropogenically through oil and gas exploration has the potential to influence climate, being a moderate absorber of infrared radiation (*2*), and ocean chemistry when it is oxidized either aerobically or anaerobically (*3*–*6*). Oceanic CH_4 has been implicated in ancient climate change [e.g., (*7*)]; however, little is known about potential future impacts (*8*). Importantly, for oceanic CH_4 to directly impact climate, CH_4 must enter the atmosphere without first being consumed by microbes in the ocean.

On 20 April 2010, a violent and tragic CH_4 discharge severed the Deepwater Horizon rig from its well. Two days later, the burning rig sank, and oil and gas began spewing into the deep Gulf of Mexico at depths of ~1.5 km until 15 July, when the well was effectively sealed. Estimates of the oil emitted during the 83 days of this disaster range from 4.1×10^6 to $4.4 \times 10^6 \pm 20\%$ (uncertainty) barrels (*9*, *10*). The corresponding emission of methane (CH_4) could be as great as 1.25×10^{10} moles (*11*) or as low as 9.14×10^9 moles (Table 1) (*12*, *13*), depending on uncertainties in the gas-to-oil ratio and net oil emission. This localized CH_4 emission is of similar magnitude to the natural release rate of CH_4 to the entire Black Sea (*14*) and provided a unique opportunity to investigate the fate of CH_4 released into the deep ocean and to understand the response of cold-adapted methanotrophic bacteria.

The sea-air CH_4 flux measured during active flow (survey area about 25 km in diameter centered on the wellhead) indicated that, even at elevated wind speeds, less than 6.8×10^5 moles (i.e., <0.01%) of the emitted CH_4 escaped to the atmosphere (*15*). The depth distributions of CH_4 in the vicinity of the wellhead measured during conditions of active flow displayed high CH_4 concentrations between 800- to 1200-m depth (*11*, *16*). This spatially consistent CH_4 distribution suggests that CH_4 remained dissolved and suspended in the deep waters between 800- to

[1]Department of Oceanography, Texas A&M University, College Station, TX 77843–3146, USA. [2]Department of Earth Science and Marine Science Institute, University of California, Santa Barbara, CA 93106, USA. [3]Geochemical and Environmental Research Group, Texas A&M University, College Station, TX 77843, USA. [4]Center for Coastal and Ocean Mapping, University of New Hampshire, Durham, NH 03824, USA.

*To whom correspondence should be addressed. E-mail: jkessler@ocean.tamu.edu (J.D.K.); valentine@geol.ucsb.edu (D.L.V.)

Seismic Detection of the Lunar Core

Renee C. Weber, Pei-Ying Lin, Edward J. Garnero, Quentin Williams and Philippe Lognonné

Science **331** (6015), 309-312.
DOI: 10.1126/science.1199375originally published online January 6, 2011